

Article

Dependence of Exchange Bias on Interparticle Interactions in Co/CoO Core/shell Nanostructures

S. Goswami ¹, P. Gupta ² , S. Nayak ², S. Bedanta ^{2,3} , Ò. Iglesias ⁴ , M. Chakraborty ¹ and D. De ^{1,5,*} 

¹ Material Science Research Lab, The Neotia University, Sarisa, D.H. Road, 24 Pgs (South) West Bengal 743368, India; e-mail@e-mail.com

² Laboratory for Nanomagnetism and Magnetic Materials (LNMM), School of Physical Sciences, National Institute of Science Education and Research (NISER), HBNI, Jatni 752050, India; e-mail@e-mail.com

³ Center for Interdisciplinary Sciences, National Institute of Science Education and Research, HBNI, Bhubaneswar, Odisha 752050, India; e-mail@e-mail.com

⁴ Dpt. Física de la Matèria Condensada and IN²UB, Facultat de Física, Universitat de Barcelona, Av. Diagonal 647, 08028 Barcelona, Spain; oscariglesias@ub.edu

⁵ Sukumar Sengupta Mahavidyalaya, State Highway 7, Keshpur, Paschim Medinipur 721150, West Bengal, India; mail@mail.com.

* Correspondence: sbedanta@niser.ac.in (S.B.); oscariglesias@ub.edu (Ò.I.); manashi.chakraborty@tnu.in (M.C.); debajyoti.de@tnu.in (D.D.)

Abstract: This article reports dependence of exchange bias (EB) effect on interparticle interactions in nanocrystalline Co/CoO core/shell structures, synthesized using conventional sol-gel technique. Analysis via powder X-Ray diffraction (PXRD) studies and transmission electron microscope (TEM) images confirm absence of crystalline phases other than core-shell Co-CoO with average particle size ≈ 18 nm. Volume fraction (φ) is varied (from 20% to 1%) by introduction of stoichiometric amount of non-magnetic amorphous silica matrix (SiO₂) which leads to a change in interparticle separation/interaction. The influence of exchange and dipolar interactions on the EB effect, caused by the variation in interparticle interaction/separation is studied for a series of Co/CoO core/shell nanoparticle systems. Studies of thermal variation of magnetization ($M - T$) and magnetic hysteresis loops ($M - H$) for the series point towards strong dependence of magnetic properties on dipolar interaction in concentrated assemblies whereas individual nanoparticle response is dominant in isolated nanoparticle systems. The analysis of the EB effect reveals a monotonic increase of coercivity (H_C) and EB field (H_E) with increasing volume fraction. When the nanoparticles are close enough and the interparticle interaction is significant, collective behavior leads to an increase in the effective antiferromagnetic (AFM) CoO shell thickness which results in high H_C , H_E . Moreover, in concentrated assemblies, the dipolar field superposes to the local exchange field and enhances the EB effect contributing as an additional source of unidirectional anisotropy.

Keywords: nanomaterials; core/shell nanostructures; exchange bias; interparticle interactions

1. Introduction

Nanoscience and nanotechnology fundamentally emerge from manipulation of matter at nanoscale and the curiosity to understand the interactions of matter at the atomic level. In nanoparticle assemblies, parameters such as size [1], surface structure [2], shape [3], agglomeration [4] or interparticle interactions [5] often influence their properties. At the same time, they lead to the emergence of enriched physico-chemical properties, which distinguish them from their bulk counterparts. Among different classes of nanomaterials, core/shell structures are fundamentally interesting because of carrying two different physico-chemical properties in one single particle at the nanoscale [6]. Though primarily, core/shell structures were synthesized to protect and stabilize the metallic core [7], advances in materials fabrication and synthesis have made core/shell structures potential

arXiv:2406.00680v1 [cond-mat.mtrl-sci] 2 Jun 2024



Citation: Dependence of Exchange Bias on Interparticle Interactions in Co/CoO Core/shell Nanostructures. *Nanomaterials* **2022**, *12*, 3159. <https://doi.org/nano12183159>

Academic Editors: Jean-Marie Nedelec and Jordi Sort

Received: 24 August 2022

Accepted: 7 September 2022

Published: 12 September 2022

Publisher's Note: MDPI stays neutral with regard to jurisdictional claims in published maps and institutional affiliations.



Copyright: © 2022 by the authors. Licensee MDPI, Basel, Switzerland. This article is an open access article distributed under the terms and conditions of the Creative Commons Attribution (CC BY) license (<https://creativecommons.org/licenses/by/4.0/>).

candidates for a myriad of new applications including targeted drug delivery [8], biomedical sensors [9], enhanced electronic properties [10] or EB effect [6]. If the core and shell are composed of two materials with different magnetic order, the interfacial region will experience a structural modification due to differences in the crystalline structures of both regions as well as a competition between the different magnetic orders favored at the core and shell. This leads to the phenomenon known as exchange bias effect [11] that was first reported by Meiklejohn and Bean as originating via unidirectional exchange anisotropy in Co-CoO (ferromagnetic (FM) - antiferromagnetic (AFM)) particles [12]. Since then, this has been intensely studied in many magnetically coupled systems such as FM/FiM (ferrimagnetic) [13], AFM/FiM [14], AFM/SG (spin-glass) [15] or FiM/SG [16].

Despite intensive experimental research in the field, there are phenomena like spontaneous exchange bias [17], EB in alloys and compounds [18,19], EB in single phase magnetically inhomogeneous materials [20] or EB in thin films [21,22] that are still drawing attention because of the urge to understand new fundamental physics as well as for the wide range of potential applications in recording media to overcome the superparamagnetic limit [23], field sensors [24], read heads [25], giant magnetoresistance (GMR) based devices [26] and many more. In this regard, tuning EB related properties by controlling variation of size [27] and thickness of core and shell [11], interparticle interactions [28] and microscopic structure of the interface of any magnetically inhomogeneous system [20] might add significant value in several application oriented phenomena. Attempts have been made to understand the underlying physics of EB mechanism when the variation of shape [29], size [14], surface composition [30], core to shell diameter ratio come into play [6], in a core/shell nanostructure. Recently, we have reported correlating experimental findings and atomistic Monte Carlo (MC) simulations showing that the variation of core and shell thickness of Co-Co₃O₄ nanostructure leads to systematic changes in the EB effect [6].

Via controlled oxidation on the surface of transition metal nanoparticles, a shell of metal oxide (generally AFM/FiM in nature) may be formed to prepare a metal/metal oxide core/shell structures [31,32]. Co/CoO is the most studied core-shell nanostructure because of its large interface energy with high EB field ($H_E \approx 1000$ Oe) compared to others [11,33]. Besides potential technological applications of Co-based nanoparticles in information storage, magnetic fluids, catalysis etc., low crystal anisotropy of Co is favorable for FM/AFM Co/CoO as a model system for EB studies [34]. Additionally, because of high AFM Néel temperature ($T_N \approx 285$ K) of CoO, followed by wide temperature range of EB effect [35], different nanostructures of the same has been revisited by researchers to understand different phenomenological models related to EB. In particular, different studies have reported how the shell thickness [35], the degree of oxidation of the shell [36], the core to shell diameter ratio [11], and the degree of dilution within non-magnetic matrix [37] affect EB in Co/CoO nanoparticles.

When particles are in close proximity, the magnetic properties of the nanoparticle assembly are mainly governed by exchange interactions between the surfaces in contact. Instead, long range dipolar interactions between the macroscopic magnetic moments of the individual particles can be relevant over a wide range of interparticle separations. As a consequence, it is expected that the thermal and field dependence of the magnetization of the assembly may be very different from that of an individual nanoparticle, giving rise to a variety of behaviors such as superparamagnetism [38,39], superspin-glass [40], and superferromagnetism [39,41] among others. Some progress has been made in recent studies of frozen ferrofluids [42], granular nanoparticles [43] and diluted magnetic systems [44].

However, to the best of our knowledge, a systematic study to understand the effect of variation of interparticle interactions on EB mechanism in core/shell nanostructure keeping the core and shell diameters fixed, has not been yet reported. In the present article, we aim to study how interparticle interactions among core/shell nanoparticles can influence the phenomenology of EB. Interparticle interactions may be varied by changing the volume fraction (φ), but a high level of dilution is required for a comparative study of their effects on

the magnetic properties [5]. Herein, we have performed a systematic and detailed study of the EB effect by changing the interparticle separation of Co/CoO core/shell nanostructures in seven different batches. Experimental findings point that collective magnetization is hindered with the increase in separation of particles via decreasing volume fraction, which leads to a monotonic reduction of coercivity (H_C) and EB field (H_E).

2. Experimental

Core/shell nanocrystalline Co/CoO is derived via controlled oxidation-reduction from nanocrystalline Co which is synthesized using conventional sol-gel technique [2]. To begin with, Co metal powder (Aldrich, 99.99% pure) is dissolved in minimum quantity of 37% nitric acid and vigorously stirred in a magnetic rotor for 12 h until the solution become transparent. Stoichiometric amount of citric acid is added in the solution and homogenized for 6 h to obtain transparent reddish solution. This ensures that all the metal ions are mixed at the atomic scale [45]. The solution is dried very slowly at room temperature for few days. To increase the evaporation rate, solution is kept inside a vacuum oven at 50° C for few days. After the solution has transformed into a gel like state, it is heated at 100° C to form a cake. This cake is then ground and heated at 600° C for 6 h in presence of continuous flow of Ar-H₂ gas (95% Ar and 5% H₂). Thus Co nanoparticles are obtained. Now, as oxidation will start from the surface, oxide shell is created via controlled oxidation at ambient temperature and the procedure is standardized after repetitive trials. The as-synthesized Co nanoparticle is then heated in open air at 200° C for 6 min to form an oxide shell over Co nanoparticle core. The shell consists of both CoO and Co₃O₄ phases (as evident from XRD pattern describe later). To synthesize desired Co-CoO, this as-synthesized core/shell sample is annealed at 250° C in a continuous flow of the same reducing gas (95% Ar and 5% H₂) for 1 hour [32]. This reduces excess oxygen from Co₃O₄ and retains only stable CoO shell on the surface of Co core. Thus finally Co/CoO core/shell nanostructure is obtained.

Variation of interparticle interactions is introduced via incorporation of non-magnetic amorphous silica matrix (SiO₂) into Co/CoO core/shell nanoparticles. Stoichiometric amount of SiO₂ is added to the as-synthesized sample and homogenized. This reduces the volume fraction and thus increase the interparticle separation leading to the simultaneous change in the interparticle interaction. Excess amount of silica is added via mechanical grinding which results in a series of samples with volume fraction (φ) as 20%, 15%, 10%, 7.5% 5%, 1% and 0.1%. This provides the platform to study the effect of variation of interparticle interactions on magnetic properties. From now on, different samples of Co/CoO embedded in SiO₂ matrix with a variation of interparticle interactions will be designated as CS-20, CS-15, CS-10, CS-7.5, CS-5, CS-1 and CS-0.1. For comparison, pure Co/CoO core/shell nanoparticle is named as CS-100. Fig. 1 demonstrate a schematic diagram, of changing volume fraction.

The structural characterization of the sample has been performed via Powder X-Ray diffraction (PXRD) pattern, recorded in a Bruker D8 Advanced Diffractometer using Cu K α ($\lambda=1.54184$ Å) radiation source with a scan speed of 0.02°/4 s. Actual shape, grain size and morphology of the NPs are assessed by Transmission Electron Microscope (TEM), equipped with an energy dispersive X-ray spectrometer (JEOL TEM, 2010). Temperature dependent dc magnetization measurements are performed via commercial SQUID magnetometer (MPMS-3). In the zero-field cooled (ZFC) protocol the sample is cooled in zero field and the magnetization is recorded in a static magnetic field during the heating cycle. In the field-cooled (FC) protocol sample is cooled in presence of a static magnetic field and magnetization measurements are performed either in heating or in cooling mode.

3. Results and discussions

3.1. Structural characterization

PXRD pattern of as-synthesized primary sample Co, intermediate sample Co-(Co₃O₄+CoO) and final product Co/CoO are recorded in the range of 30°-80° at 300 K and are depicted in Fig. 2(a)-(c). An elaborate Rietveld refinement has been performed on the diffrac-

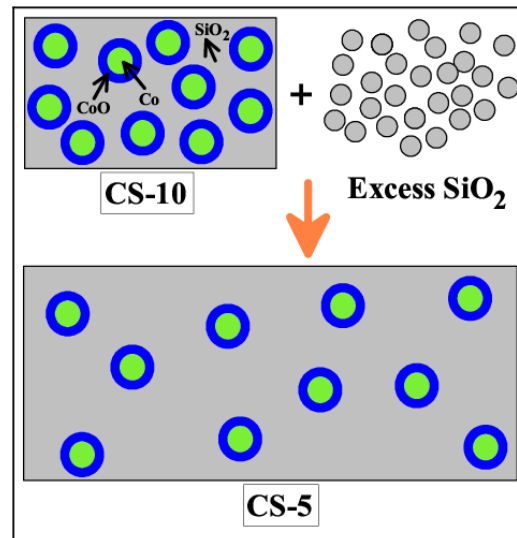


Figure 1. Schematic diagram representing change in volume fraction of Co-CoO nanoparticles from 10% to 5% by introducing excess silica matrix in the system.

Table 1. Lattice and refinement parameters

Sample	Structure	a (Å)	R_p (%)	R_{wp} (%)	χ^2	D (PXRd)(nm)	D (TEM)(nm)
Co	Fm3m	3.558(0.004)	1.8399	2.3351	1.1762	26	12.22(0.09)
Co/(Co ₃ O ₄ +CoO)	Fm3m (Co)	3.551(0.002)					
	$Fd\bar{3}m$ (Co ₃ O ₄)	8.093(0.002)	1.6499	2.0905	1.0839	29	16.57(0.27)
	Fm3m (CoO)	4.260(0.001)					
Co/CoO	Fm3m (Co)	3.545(0.001)	1.3173	1.6411	1.1198	30	17.54(0.02)
	Fm3m (CoO)	4.255(0.001)					

tion patterns using MAUD (materials analysis using diffraction) software, considering face-centered $Fm\bar{3}m$ space group for Co, CoO and $Fd\bar{3}m$ for Co₃O₄. A close match of experimental data and computed curves are noticed as indicated by the difference plots at the bottom of Figs. 2(a)–(c). Fig. 2(a) corresponds to Co nanoparticle only whereas Fig. 2(b) represents the XRD pattern of as synthesized Co-(Co₃O₄+CoO) developed after oxidation treatment Co nanoparticles in open air. Co-(Co₃O₄+CoO) demonstrate the characteristic peaks of Co, Co₃O₄ and CoO, which are in accordance with the JCPDS data (15-0806), (43-1003) and (43-1004), respectively. Weight percentage of different compositions present in this intermediate sample is Co:Co₃O₄:CoO ≈ 26:68:6, as evident from the refinement results. Fig. 2(c) shows the peak positions corresponding to Co and CoO phases only. Proper indexing of all the peaks in Fig. 2(c) rules out the possibility of presence of any other secondary phases or impurity in the final product Co/CoO. Refinement also suggests that the weight percentage of Co:CoO ≈ 20:80. This suggests, controlled oxidation-reduction converts Co₃O₄ into stable CoO phase [32]. Vertical bars at the bottom of Figs. 2(a)–(c) in three different colors correspond to different phases (Co, Co₃O₄ and CoO). Information extracted from the Rietveld refinement such as, lattice parameters, atomic positions, refined parameters (R_p , R_{wp} and χ^2 as shown in Table 1), bond angles are in acceptable range and are in close agreement with the recent results [46–48]. Increase in average crystallite sizes (D) of the three sample, as determined by modified Scherrer’s formula [49,50] from the corresponding PXRd patterns, commensurate with the heat treatment (see Table 1).

To investigate the actual size and morphology of the samples and its procedural changes with synthesis, TEM micrographs are studied for all the three samples. Figs 3(a–b), (e–f) and (i–j) depict spherical nanoparticles for Co, Co-(Co₃O₄+CoO) and Co/CoO, respectively. Insets of Figs. 3(a), (e) and (i) represent the histograms of particle size

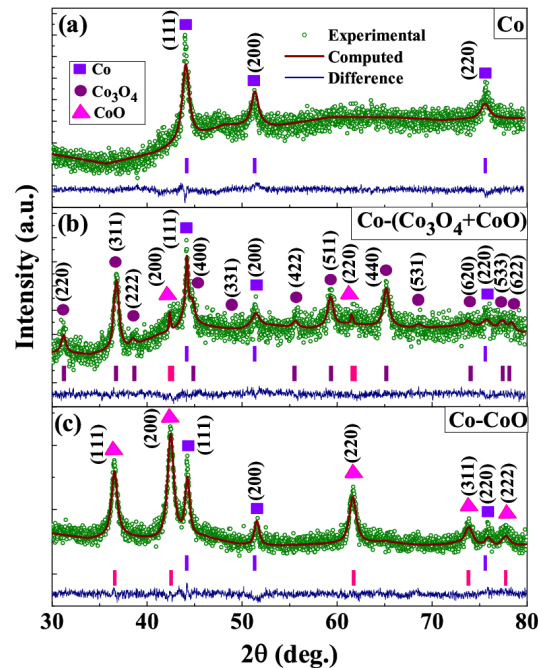


Figure 2. PXRD pattern of (a) Co nanoparticle, (b) Co-(Co₃O₄+CoO), after heating the Co nanoparticle in open air and (c) Co/CoO core/shell structure. Solid continuous curves are the fits using Rietveld refinement and the lowermost plots in each panel are the residuals. Vertical bars correspond to different peak positions corresponding to different crystallites.

distributions of the samples, fitted with log normal distribution function. Fittings result average particle sizes that are found to be ≈ 12 nm for Co ($\sigma_{\log}=0.15$), ≈ 15 nm for Co-(Co₃O₄+CoO) ($\sigma_{\log}=0.18$) and ≈ 16 nm for Co/CoO ($\sigma_{\log}=0.23$), respectively. Here too, the gradual increase in particle sizes supports the findings of the PXRD studies and is in accordance with the heat treatment. Figs. 3(c), (g) and (k) represent the high resolution (HR) TEM images of the samples revealing formation of high crystallinity up to the edges of the particles. Lattice plane spacing of (111) plane for Co, (311) for Co₃O₄ and (111) for CoO are observed in different HR-TEM images which corresponds to the formation of core/shell structure. Selected area electron diffraction (SAED) patterns of the nanoparticles are presented in Figs. 3(d), (h) and (l) where planes corresponding to Co, Co₃O₄ and CoO are observed. Findings support the PXRD studies and no impurity plane is noted. The results obtained from two different techniques replicate almost similar results, indicating the purity of the samples. Then, the duly characterized core/shell Co/CoO nanoparticles undergo a treatment of variation of interparticle interactions via introduction of SiO₂ in desired limit and samples with different volume fractions are prepared for detailed magnetic characterization.

3.2. Magnetic characterization

3.2.1. ZFC-FC thermal dependence

To understand the effect of interparticle interactions on the magnetic behavior of as synthesized Co/CoO nanoparticles with different volume fractions, thermal variation of magnetization ($M - T$) in ZFC and FC modes in an applied field of 100 Oe field were measured and the results are shown Fig. 4 for CS-10, CS-5 and CS-1 samples as representative of the series. The general trends of $M - T$ curves is similar for the three samples, showing irreversibility up to the maximum measured temperature of 320 K [51] and suggesting that the blocking temperature is above this value which is reasonable given the relatively big nanoparticle sizes. All the curves decrease monotonously below 320 K, but ZFC curves show a subtle but noticeable anomaly at ≈ 290 K, which corresponds to the Néel temperature (T_N) of the AFM CoO shell [11,34,35] and explains the steeper decrease

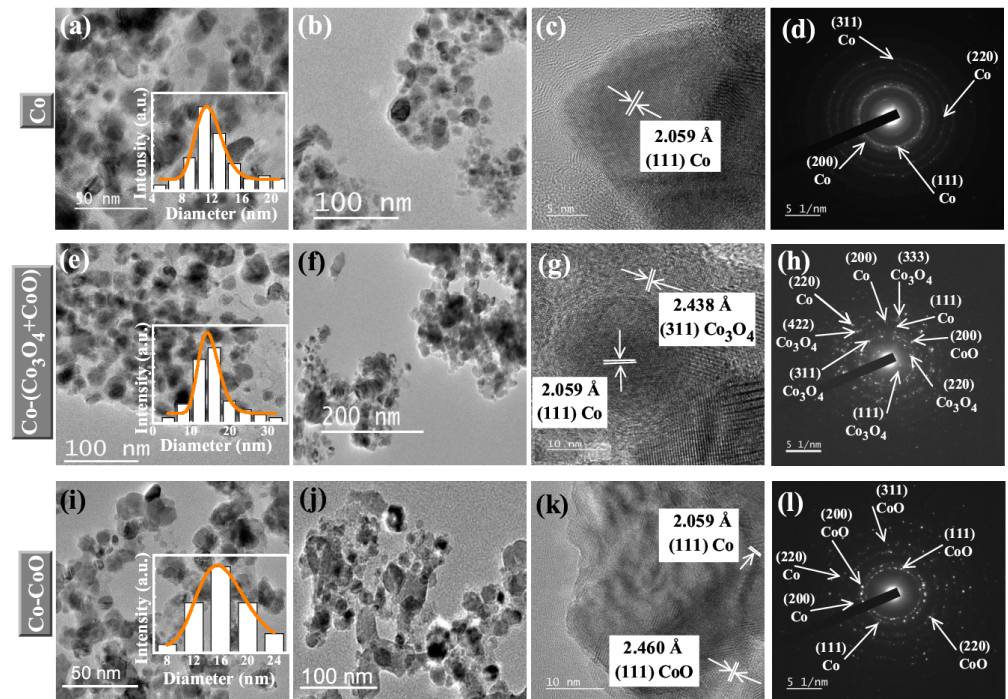


Figure 3. TEM images of Co ((a)&(b)), Co-(Co₃O₄+CoO) ((e)&(f)) and Co/CoO ((i)&(j)) show well dispersed particles with distribution of particle sizes. Insets of (a), (e) and (i) depict the histograms of particle sizes, fitted with log-normal distribution function. (c), (g) and (k) HR TEM images, highlighting plane spacings of Co, Co₃O₄ and CoO. (d), (h) and (l) correspond to SAED pattern of the three samples, indicating different crystalline planes which are in accordance with the PXRD pattern.

of the magnetization below this temperature. No anomaly is observed at the ordering temperature of Co₃O₄ (≈ 40 K), confirming the absence of this phase as also evidenced by PXRD. We notice a sudden magnetization increase below 12 K for all the samples, generally known as Curie-tail like behavior [52], that is usually observed in systems with broken spin chains or paramagnetic like impurities [53]. Recent reports suggest that the presence of oxygen atoms in the CoO shell generate holes that break the infinite lattice chain and thus can lead to the low temperature up-tail [54]. The Curie-tail is more pronounced as the volume fraction increases, indicating that upon dilution collective magnetic effects diminish leading to a reduction of the Curie-tail. Curves of samples with increasing ϕ in Fig. 4 display a progressive decrease of the magnitude of the magnetization that is a first evidence that interparticle interactions change the magnetic behavior of the core/shell nanoparticles.

3.2.2. ZFC Hysteresis loops

In order to study the influence of interactions on the reversal by a magnetic field, $M - H$ hysteresis loops for all the seven samples with different ϕ have been measured in between ± 50 kOe magnetic fields after cooling the samples from 300 K to 4 K in zero field (ZFC), as displayed in Fig. 5. For the most diluted samples (CS-0.1, CS-1), the loops do not saturate even at 50 kOe. The observed high field quasi linear response characteristic of a SPM is a typical signature of a disordered system. In these cases, the response to a magnetic field as reflected in the loops must come from intrinsic properties of an individual core/shell particles. Surface spins may present frustration due to broken links or lack of coordination, and increased surface anisotropy [55], which distinguish them from those at inner regions of the shell that are pinned by the coupling to core spins and do not contribute to the magnetic response [34]. Therefore, the absence of saturation at low temperature with lower ϕ can be attributed to the progressive alignment of the outermost layer of the AFM shell spins towards the core magnetization.

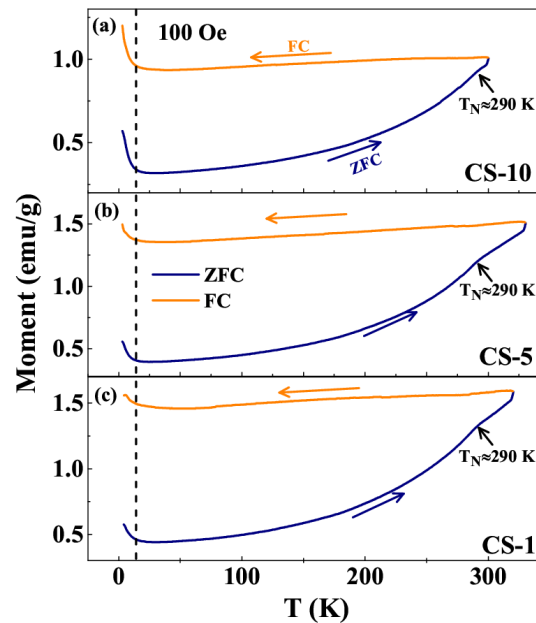


Figure 4. Thermal dependence of the ZFC and FC magnetization of samples (a) CS-10, (b) CS-5 and (c) CS-1, at 100 Oe. Anomalies evident near 290 K correspond to the Néel temperature (T_N) of CoO. In the low temperature region, a Cuire-tail like behavior is observed for all the samples.

However, this behavior changes to $M - H$ loops that saturate towards lower values of the magnetization as the interparticle separation is decreased. This can be seen in Fig. 5 for samples CS-5 to CS-20, where in the latter the magnetization saturates already at 10 kOe to $M_S \approx 27$ emu/g, whereas for the most diluted system CS-0.1 $M_S \approx 111$ emu/g at 50 kOe field. As φ increases, the mean interparticle separation decreases and dipolar interactions become more relevant. Thus, in the more concentrated assemblies, the magnetic behavior is dominated by collective effects induced by dipolar interactions of the FM Co cores, the $M - H$ loops display the typical shape of a superferromagnetic (SFM) system [39] and the SPM contribution coming from the individual nanoparticle response is suppressed. Assuming that dipolar interactions arise from the FM cores (neglecting the AF shell contribution to the total magnetization), typical dipolar energies between two Co particles separated by a distance d twice the shell thickness can be evaluated as $E_{\text{dip}} = \frac{\mu_0 M_s^2 V^2}{4\pi d^3} \approx 1220$ K, to be compared with anisotropy energy $E_{\text{ani}} = KV \approx 3030$ K, which qualifies our samples with higher volume fraction as governed by collective dipolar behavior [56,57]. The overall behavior is consistent with the changes in the magnetization in the low temperature region of the $M - T$ curves shown in Fig. 4.

3.2.3. Exchange bias

The influence of interactions on the EB effect was evidenced by recording also hysteresis loops after cooling in an applied field $H_{\text{cool}}=10$ kOe. The central portions of the loops are shown by red dashed lines in Figs. 6(a-h); ZFC loops are displayed in the same figure as black solid lines. For comparison, the $M - H$ loop of CS-100, (Co/CoO without SiO₂) is also included and insets in the corresponding panels show the $M - H$ loops in full scale. All loops after FC show a notable shift contrary to the cooling field direction as indicated by the arrows with a concomitant increase in the coercive field with respect to the one measured under ZFC conditions [58]. The fact that the shift is observed even for the most diluted sample (CS-0.1) asserts the existence of a unidirectional anisotropy, originated by the freezing of the AF shell spins, and that the resulting EB effect is induced at the individual particle level [18,19]. The EB field (H_E) and coercivity (H_C) have been determined as $H_E = |H_2 + H_1|/2$ and $H_C = |(H_2 - H_1)|/2$; where H_1 and H_2 are the coercivities of the decreasing and increasing field branches respectively [6]. The resulting dependence

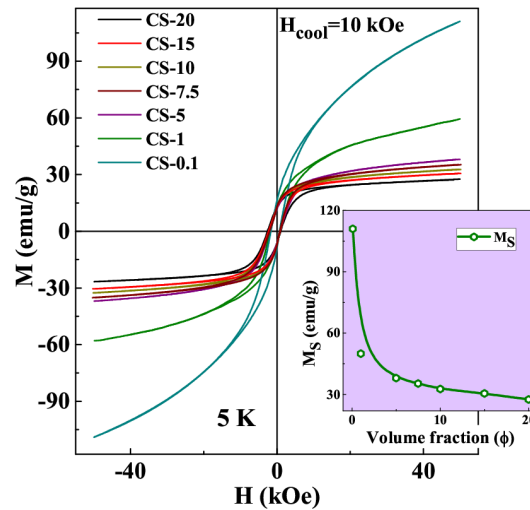


Figure 5. $M - H$ loops of samples CS-20, CS-15, CS-10, CS-7.5, CS-5, CS-1, CS-0.1 measured in ZFC mode. Inset shows the variation of M_S with volume fraction (ϕ).

of H_E and H_C with the volume fraction ϕ in the different samples is depicted in Fig. 6(i), which shows a monotonic increase of both quantities with increasing ϕ , i.e. increasing interparticle interactions. In going from CS-0.1 to CS-20 H_C and H_E change from 1191 Oe to 1793 and from 473 to 800, respectively. Since the samples with different ϕ are derived from the same mother sample (CS-100) by introduction of additional SiO_2 , it can be assumed that the contribution to the loop shift coming from the exchange coupling at the interfacial region of the individual particles is the same for all of them. Therefore, the reason for the observed notably higher values H_C , H_E at higher concentrations must have its origin in the decrease of interparticle distance at higher ϕ . On the one hand, it can be argued that when CoO shells come close to each other, the effective thickness of AFM shell increases, leading to an increase in magnetic coupling and coercive field between the FM core and AFM shell as argued in [37]. However, this effect could only partially explain the observations. Recent MC simulations of a simplified macrospin model of core/shell nanoparticle assemblies [59,60] have shown that the EB field is influenced by both direct interparticle exchange and dipolar interactions, whose contributions could be separately evaluated. Simulation results were in good agreement with experimental results showing an increase of H_E in powder samples compared to diluted ferrofluids [60,61].

We believe that, due to the higher core sizes and shell thicknesses of our samples, the reason behind the EB enhancement is the increase of the dipolar fields felt by the individual particles as the particles approach to each other. In an individual core/shell nanoparticle, the loop shift is related to the local exchange field created by the uncompensated spins at the interface [62] that adds in opposite directions at the decreasing and increasing field loop branches and generates a unidirectional anisotropy. Our situation bears similarities with the dipole-induced EB model proposed in [63] to explain EB in AFM/FM thin films separated by an interface layer. When the particle is in an assembly, the dipolar field generated by the rest of particles superposes to the local exchange field and acts as an additional source of unidirectional anisotropy that enhances the EB effect. In order to reinforce this interpretation, we will now give an estimation of typical dipolar fields that can be found in SFM samples, using an argument that was also employed to explain the shift in energy barrier distributions due to dipolar interactions in [64]. Let us consider a Co core of diameter $D = 18$ nm. A rough estimate of the dipolar field felt at a distance two times the typical shell thickness $d = 24$ nm can be obtained as $H_{dip} = \frac{\mu_0}{4\pi} \frac{M_S V}{d^3} \approx 110$ Oe. This is of the correct order of magnitude of the increase in 327 Oe observed for $\phi = 20$ in Fig.6(i), if we consider that the H_{dip} acting on a particle receives contributions from several neighbors and that their magnetizations may not be aligned.

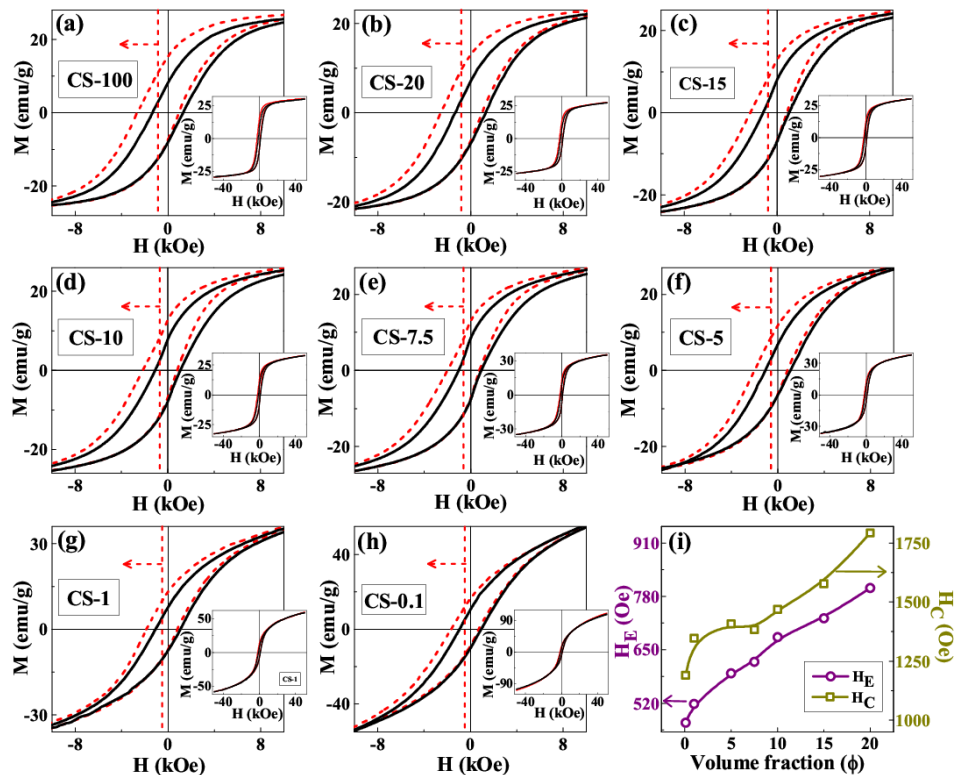


Figure 6. (a)–(e) Central portions of the ZFC (solid line) and in the FC ($H_{cool}=10$ kOe, dashed line) $M-H$ loops recorded at 4 K for CS-100, CS-20, CS-15, CS-10, CS-7.5 CS-5, CS-1 and CS-0.1. Full scale $M-H$ loops are depicted in the corresponding insets. (i) Variation of coercivity (H_C) and EB field (H_E) with change in volume fraction (ϕ).

To study the dependence of H_C and H_E with cooling field (H_{cool}), $M-H$ loops at different fields ($H_{cool}=0.2, 0.5, 5, 10, 25, 50$ kOe) were recorded in between ± 50 kOe after cooling the sample from 300 to 4 K in FC mode. The results are shown in Fig. 7(a) for the CS-5 sample as representative of the series. Hysteresis loops at $H_{cool} = 10$ kOe were also recorded for a wide temperature range (5–250 K) to study the nature of EB for CS-5 at different temperatures (refer Fig. 7(b)). The variation of the calculated parameters H_E and H_C with H_{cool} and T are presented in Figs. 7(c) and (d), respectively. Both H_C and H_E increase with H_{cool} and almost become saturated near 10 kOe. Then, we can exclude that observed phenomenology can be attributed to a minor loop effect, in accordance with recent reports [6,20]. Fig. 7(d) demonstrates a monotonic decrease of H_C and H_E with increase in temperature. H_E almost vanishes at 250 K which is close to the Néel temperature of CoO shell. Decrease of H_E with T may be due to the loss of interface coupling between Co core and CoO shell caused by the increase in thermal fluctuations and the decrease in AFM anisotropy with increase in temperature [65,66].

4. Conclusions

Co nanoparticle has been synthesized using conventional sol-gel technique with average particle size 12 nm. CoO shell has been formed over the Co nanoparticle via controlled oxidation-reduction which results in the formation of core/shell nanoparticles (Co/CoO) with average particle sizes 18 nm. Samples were characterized by PXRD and TEM analysis. Coexistence of Co and CoO phases are confirmed without a very regular core/shell structure. Interparticle interaction/separation among the individual nanoparticles has been tuned by changing the volume fraction via introduction of additional SiO_2 matrix. Notably, different trends in the thermal dependence of the magnetization are observed between samples with different interparticle interactions. Starting from the most concentrated sample, a gradual decrease in coercivity and increase in non-saturation tendency was obtained with

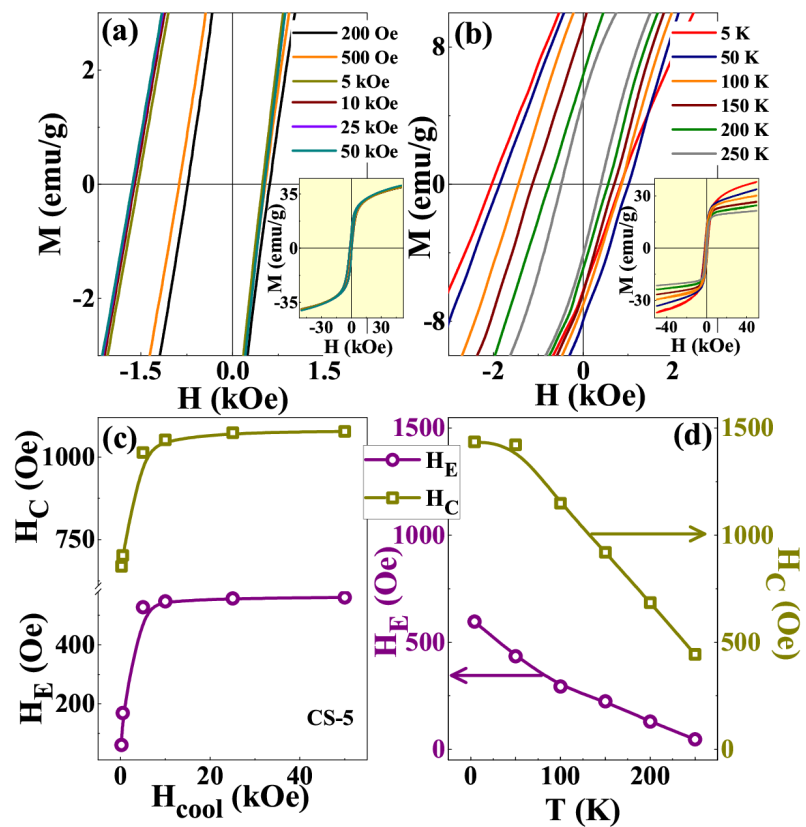


Figure 7. (a) Low field region of $M - H$ loops of CS-5 recorded at 4 K in between ± 50 kOe for $H_{cool} = 0.2, 0.5, 5, 10, 25$ and 50 kOe. Inset of (a) shows the corresponding $M - H$ loops in full scale. (b) $M - H$ loops of CS-5 measured at different temperatures in FC mode at $H_{cool} = 10$ kOe. Inset of (b) shows the corresponding $M - H$ loops in full scale. (c) and (d) Variation of H_E and H_C with change in cooling field and temperature, respectively.

the incorporation of the non-magnetic matrix from the $M - H$ loops, demonstrating the change from SPM response due to individual nanoparticles to a SFM collective behavior as the interparticle interactions increased. Our study of EB effects, have revealed that H_C , H_E and M_S can be tuned monotonously with the increase of the volume fraction of the core/shell nanoparticles. We have given an interpretation of the nature of the variations of H_C and H_E with φ , linking them to changes in interfacial coupling of FM core and AFM shell and increase of the local fields felt by the Co cores as a consequence of increasing dipolar interactions when the distance between the nanoparticles is decreased.

It is worth noticing that the understanding of the variation of EB related parameters with interparticle interactions along with our previous findings of variation of EB with core to shell diameter ratio [6] provide us a platform to tune or have a deep control over the EB related phenomenon and parameters of core/shell structures to explore application oriented device fabrication. In this study, Co/CoO nanostructure has been chosen as a representative of metal/metal oxide (FM/AFM) system revealing EB effect. The dependency of H_C and H_E reported here with interparticle interaction, may be considered as a general phenomenon after similar studies with core/shell nanoparticles of similar and different compositions. Finally, we may conclude that, though the EB phenomenon was discovered about 70 years ago, there are still many out of the box origins of EB mechanism that differ from the conventional knowledge of pinning mechanism at the interface between materials with different magnetic ordering. Full understanding of these new underlying mechanisms in EB assemblies will necessitate further experimental studies and will need to improve current theoretical frameworks that can incorporate collective effects due to dipolar interactions.

Author Contributions: Conceptualization, D.D.; methodology, S.G., P.G., S.N., S.B., M.C. and D.D.; validation, S.B., Ò.I. and D.D.; formal analysis, S.G., P.G., S.N., S.B., Ò.I., M.C. and D.D.; investigation, S.G., P.G., S.N., S.B., M.C. and D.D.; data curation, S.G., P.G. and S.N.; writing—original draft preparation, S.G., P.G., S.N., S.B., Ò.I., M.C. and D.D.; writing—review and editing, S.B., Ò.I., M.C. and D.D.; visualization, S.B., D.D. and Ò.I.; supervision, S.B., M.C. and D.D.; project administration, D.D.; funding acquisition, S.B., Ò.I., M.C. and D.D. All authors have read and agreed to the published version of the manuscript.

Funding: This work is an outcome of collaborative research of Material Science Research Lab, The Neotia University and Laboratory for Nanomagnetism and Magnetic Materials, NISER, Bhubaneswar. D. De, M. Chakraborty and S. Goswami thank SERB Project EMR/2017/001195 for financial support. S. Bedanta wishes to thank DAE for financial support. Ò. Iglesias thanks Spanish MINECO projects PGC2018-097789-B-I00, PID2019-109514RJ-I00 and the European Union FEDER funds.

Acknowledgments: D. De, M. Chakraborty and S. Goswami thank The Neotia University authority & Sukumar Sengupta Mahavidyalaya for their cooperation and encouragement. All authors thank, Prof. N. Sarkar, The Neotia University, Dr. S. Dey, Purulia Polytechnic, W.B., India, Mr. A. Maity of The Neotia University and Dr. A. Banerjee, IACS Kolkata for research support.

Conflicts of Interest: The authors declare no conflict of interest.

References

1. He, X.; Zhong, W.; Au, C.T.; Du, Y. Size dependence of the magnetic properties of Ni nanoparticles prepared by thermal decomposition method. *Nanoscale Research Lett.* **2013**, *8*, 446. <https://doi.org/10.1186/1556-276X-8-446>.
2. Goswami, S.; Manna, P.K.; Bedanta, S.; Dey, S.K.; Chakraborty, M.; De, D. Surface driven exchange bias in nanocrystalline CoCr_2O_4 . *J. Phys. D: Appl. Phys.* **2020**, *53*, 305303. <https://doi.org/10.1088/1361-6463/ab87c7>.
3. Auvinen, S.; Alatalo, M.; Haario, H.; Jalava, J.P.; Lamminmäki, R.J. Size and Shape Dependence of the Electronic and Spectral Properties in TiO_2 Nanoparticles. *J. Phys. Chem. C* **2011**, *115*, 8484. <https://doi.org/10.1021/jp112114p>.
4. Ashraf, M.A.; Peng, W.; Zare, Y.; Rhee, K.Y. Effects of Size and Aggregation/ Agglomeration of Nanoparticles on the Interfacial/Interphase Properties and Tensile Strength of Polymer Nanocomposites. *Nanoscale Research Lett.* **2018**, *13*, 214. <https://doi.org/10.1186/s11671-018-2624-0>.
5. Papaefthymiou, G.C.; Devlin, E.; Simopoulos, A.; Yi, D.K.; Riduan, S.N.; Lee, S.S.; Ying, J.Y. Interparticle interactions in magnetic core/shell nanoarchitectures. *Phys. Rev. B* **2009**, *80*, 024406. <https://doi.org/10.1103/PhysRevB.80.024406>.
6. De, D.; Iglesias, Ò.; Majumdar, S.; Giri, S. Probing core and shell contributions to exchange bias in Co/ Co_3O_4 nanoparticles of controlled size. *Phys. Rev. B* **2016**, *94*, 184410. <https://doi.org/10.1103/PhysRevB.94.184410>.

7. Chaudhuri, R.G.; Paria, S. Core/Shell Nanoparticles: Classes, Properties, Synthesis Mechanisms, Characterization, and Applications. *Chem. Rev.* **2012**, *112*, 2373. <https://doi.org/10.1021/cr100449n>.
8. Schärfl, W. Current directions in core-shell nanoparticle design. *Nanoscale* **2010**, *2*, 829. <https://doi.org/10.1039/c0nr00028k>.
9. Al-Ogaidi, I.; Gou, H.; Al-kazaz, A.K.A.; Aguilar, Z.P.; Melconian, A.K.; Zheng, P.; Wu, N. A goldsilica core-shell nanoparticle-based surface-enhanced Raman scattering biosensor for label-free glucose detection. *Anal. Chim. Acta* **2014**, *811*, 76. <https://doi.org/10.1016/j.aca.2013.12.009>.
10. Cha, S.K.; Mun, J.H.; Chang, T.; Kim, S.Y.; Kim, J.Y.; Jin, H.M.; Lee, J.Y.; Shin, J.; Kim, K.H.; Kim, S.O. Au-Ag Core-Shell Nanoparticle Array by Block Copolymer Lithography for Synergistic Broadband Plasmonic Properties. *ACS Nano* **2015**, *9*, 5536. <https://doi.org/10.1021/acs.nano.5b01641>.
11. Feyngenson, M.; Yiu, Y.; Kou, A.; Kim, K.S.; Aronson, M.C. Controlling the exchange bias field in Co core/CoO shell nanoparticles. *Phys. Rev. B* **2010**, *81*, 195445. <https://doi.org/10.1103/PhysRevB.81.195445>.
12. Meiklejohn, W.H.; Bean, C.P. New Magnetic Anisotropy. *Phys. Rev.* **1956**, *102*, 1413. <https://doi.org/10.1103/PhysRev.102.1413>.
13. Vasilakaki, M.; Trohidou, K.N. Numerical study of the exchange-bias effect in nanoparticles with ferromagnetic core/ ferrimagnetic disordered shell morphology. *Phys. Rev. B* **2009**, *79*, 144402. <https://doi.org/10.1103/PhysRevB.79.144402>.
14. Salazar-Alvarez, G.; Sort, J.; Suriñach, S.; Baró, M.D.; Nogués, J. Synthesis and Size-Dependent Exchange Bias in Inverted Core-Shell MnO|Mn₃O₄ Nanoparticles. *J. Am. Chem. Soc.* **2007**, *129*, 9102. <https://doi.org/10.1021/ja0714282>.
15. Sahoo, R.C.; Giri, S.K.; Dasgupta, P.; Poddar, A.; Nath, T.K. Exchange bias effect in ferromagnetic LaSrCoMnO₆ double perovskite: consequence of spin glass-like ordering at low temperature. *J. Alloys and Compounds* **2016**, *658*, 1003. <https://doi.org/10.1016/j.jallcom.2015.11.025>.
16. Wang, H.; Zhu, T.; Zhao, K.; Wang, W.N.; Wang, C.S.; Wang, Y.J.; Zhan, W.S. Surface spin glass and exchange bias in Fe₃O₄ nanoparticles compacted under high pressure. *Phys. Rev. B* **2004**, *70*, 092409. <https://doi.org/10.1103/PhysRevB.70.092409>.
17. Giri, S.K.; Sahoo, R.C.; Dasgupta, P.; Poddar, A.; Nath, T.K. Giant spontaneous exchange bias effect in Sm_{1.5}Ca_{0.5}CoMnO₆ perovskite. *J. Phys. D: Appl. Phys.* **2016**, *49*, 165002. <https://doi.org/10.1088/0022-3727/49/16/165002>.
18. Giri, S.; Patra, M.; Majumdar, S. Exchange bias effect in alloys and compounds. *J. Phys.: Condens. Matter* **2011**, *23*, 073201. <https://doi.org/10.1088/0953-8984/23/7/073201>.
19. Nogués, J.; Sort, J.; Langlais, V.; Skumryev, V.; Suriñach, S.; Muñoz, J.S.; Baró, M.D. Exchange bias in nanostructures. *Phys. Rep.* **2005**, *422*, 65. <https://doi.org/10.1016/j.physrep.2005.08.004>.
20. Goswami, S.; Gupta, P.; Bedanta, S.; Chakraborty, M.; De, D. Coexistence of exchange bias and memory effect in nanocrystalline CoCr₂O₄. *J. Alloys and Compounds* **2022**, *890*, 161916. <https://doi.org/10.1016/j.jallcom.2021.161916>.
21. Nayak, S.; Manna, P.K.; Vijayabaskaran, T.; Singh, B.B.; Chelvane, J.A.; Bedanta, S. Exchange bias in Fe/ Ir₂₀ Mn₈₀ bilayers: Role of spin-glass like interface and bulk' antiferromagnet spins. *J. Magn. Magn. Mater.* **2020**, *499*, 166267. <https://doi.org/10.1016/j.jmmm.2019.166267>.
22. Nayak, S.; Manna, P.K.; Singh, B.B.; Bedanta, S. Effect of spin glass frustration on exchange bias in NiMn/CoFeB bilayers. *Phys. Chem. Chem. Phys.* **2021**, *23*, 6481. <https://doi.org/10.1039/d0cp05726f>.
23. Skumryev, V.; Stoyanov, S.; Zhang, Y.; Hadjipanayis, G.; Givord, D.; Nogués, J. Beating the superparamagnetic limit with exchange bias. *Nature* **2003**, *423*, 850. <https://doi.org/10.1038/nature0168>.
24. Sharma, P.P.; Albisetti, E.; Monticelli, M.; Bertacco, R.; Petti, D. Exchange Bias Tuning for Magnetoresistive Sensors by Inclusion of Non-Magnetic Impurities. *Sensor* **2016**, *16*, 1030. <https://doi.org/10.3390/s16071030>.
25. Nogués, J.; Schuller, I.K. Exchange bias. *J. Magn. Magn. Mater.* **1999**, *192*, 203. [https://doi.org/10.1016/S0304-8853\(98\)00266-2](https://doi.org/10.1016/S0304-8853(98)00266-2).
26. Aktas, K.Y.; Kocaman, B.; Basaran, A.C. Magnetic and Electrical (GMR) Properties of Rh(IrMn)/Co/Cu/Ni(Py) Multilayered Thin Films. *Journal of Superconductivity and Novel Magnetism* **2020**, *33*, 2093. <https://doi.org/10.1007/s10948-020-05464-8>.
27. Huang, X.H.; Ding, J.F.; Zhang, G.Q.; Hou, Y.; Yao, Y.P.; Li, X.G. Size-dependent exchange bias in La_{0.25}Ca_{0.75}MnO₃ nanoparticles. *Phys. Rev. B* **2008**, *78*, 224408. <https://doi.org/10.1103/PhysRevB.78.224408>.
28. Das, S.; Majumdar, S.; Giri, S. Multifunctional properties of CoNi alloy embedded in the SiO₂ host: Role of interparticle interaction. *J. Solid State Chem.* **2011**, *184*, 2215. <https://doi.org/10.1016/j.jssc.2011.06.038>.
29. Dimitriadis, V.; Kechrakos, D.; Chubykalo-Fesenko, O.; Tsiantos, V. Shape-dependent exchange bias effect in magnetic nanoparticles with core-shell morphology. *Phys. Rev. B* **2015**, *92*, 064420. <https://doi.org/10.1103/PhysRevB.92.064420>.
30. Obaidat, I.M.; Nayek, C.; Manna, K.; Bhattacharjee, G.; Al-Omari, I.A.; Gismelseed, A. Investigating Exchange Bias and Coercivity in Fe₃O₄-γ-Fe₂O₃ Core-Shell Nanoparticles of Fixed Core Diameter and Variable Shell Thicknesses. *Nanomaterials* **2017**, *7*, 415. <https://doi.org/10.3390/nano7120415>.
31. Giri, S.; Ganguli, S.; Bhattacharya, M. Surface oxidation of iron nanoparticles. *Appl. Surf. Sci.* **2001**, *182*, 345. [https://doi.org/10.1016/S0169-4332\(01\)00446-9](https://doi.org/10.1016/S0169-4332(01)00446-9).
32. Zhang, L.; Hu, P.; Zhao, X.; Tian, R.; Zou, R.; Xia, D. Controllable synthesis of core-shell Co@CoO nanocomposites with a superior performance as an anode material for lithium-ion batteries. *J. Mater. Chem.* **2011**, *21*, 18279. <https://doi.org/10.1039/C1JM12990B>.
33. González, J.A.; Andrés, J.P.; Antón, R.L.; De Toro, J.A.; Normile, P.S.; Muñoz, P.; Riveiro, J.M.; Nogués, J. Maximizing exchange-bias in Co/CoO core/shell nanoparticles by lattice matching between the shell and the embedding matrix. *Chem. Mater.* **2017**, *29*, 5200. <https://doi.org/10.1021/acs.chemmater.7b00868>.

34. Simeonidis, K.; Martinez-Boubeta, C.; Iglesias, Ò.; Cabot, A.; Angelakeris, M.; Mourdikoudis, S.; Tsiaoussis, I.; Delimitis, A.; Dendrinou-Samara, C.; Kalogirou, O. Morphology influence on nanoscale magnetism of Co nanoparticles: Experimental and theoretical aspects of exchange bias. *Phys. Rev. B* **2011**, *84*, 144430. <https://doi.org/10.1103/PhysRevB.84.144430>.
35. Tracy, J.B.; Weiss, D.N.; Dinega, D.P.; Bawendi, M.G. Exchange biasing and magnetic properties of partially and fully oxidized colloidal cobalt nanoparticles. *Phys. Rev. B* **2005**, *72*, 064404. <https://doi.org/10.1103/PhysRevB.72.064404>.
36. Kovylyna, M.; Muro, M.G.D.; Konstantinović, Z.; Varela, V.; Iglesias, Ò.; Labarta, A.; Batlle, X. Controlling exchange bias in Co–CoO_x nanoparticles by oxygen content. *Nanotechnology* **2009**, *20*, 175702. <https://doi.org/10.1088/0957-4484/20/17/175702>.
37. Nogués, J.; Skumryev, V.; Sort, J.; Stoyanov, S.; Givord, D. Shell-Driven Magnetic Stability in Core-Shell Nanoparticles. *Phys. Rev. Lett.* **2006**, *97*, 157203. <https://doi.org/10.1103/PhysRevLett.97.157203>.
38. Bean, C.P.; Livingston, J.D. Superparamagnetism. *J. Appl. Phys.* **1959**, *30*, S120. <https://doi.org/10.1063/1.2185850>.
39. Bedanta, S.; Kleemann, W. Supermagnetism. *J. Phys. D: Appl. Phys.* **2008**, *42*, 013001. <https://doi.org/10.1088/0022-3727/42/1/013001>.
40. Chen, X.; Bedanta, S.; Petravic, O.; Kleemann, W.; Sahoo, S.; Cardoso, S.; Freitas, P.P. Superparamagnetism versus superspin glass behavior in dilute magnetic nanoparticle systems. *Phys. Rev. B* **2005**, *72*, 214436. <https://doi.org/10.1103/PhysRevB.72.214436>.
41. Bedanta, S.; Eimüller, T.; Kleemann, W.; Rhensius, J.; Stromberg, F.; Amaladass, E.; Cardoso, S.; Freitas, P.P. Overcoming the Dipolar Disorder in Dense CoFe Nanoparticle Ensembles: Superferromagnetism. *Phys. Rev. Lett.* **2007**, *98*, 176601. <https://doi.org/10.1103/PhysRevLett.98.176601>.
42. Luo, W.; Nagel, S.R.; Rosenbaum, T.F.; Rosensweig, R.E. Dipole Interactions with Random Anisotropy in a Frozen Ferrofluid. *Phys. Rev. Lett.* **1991**, *67*, 2721. <https://doi.org/10.1103/PhysRevLett.67.2721>.
43. Moscoso-Londoño, O.; Tancredi, P.; Muraca, D.; Zélis, P.M.; Coral, D.; Fernández van Raap, M.B.; Wolff, U.; Neu, V.; Damm, C.; de Oliveira, C.L.P.; et al. Different approaches to analyze the dipolar interaction effects on diluted and concentrated granular superparamagnetic systems. *J. Magn. Magn. Mater.* **2017**, *428*, 105. <https://doi.org/10.1016/j.jmmm.2016.12.019>.
44. Vestal, C.R.; Song, Q.; Zhang, Z.J. Effects of Interparticle Interactions upon the Magnetic Properties of CoFe₂O₄ and MnFe₂O₄ Nanocrystals. *J. Phys. Chem. B* **2004**, *108*, 18222. <https://doi.org/10.1021/jp0464526>.
45. De, K.; Ray, R.; Panda, R.N.; Giri, S.; Nakamura, H.; Kohara, T. The effect of Fe substitution on magnetic and transport properties of LaMnO₃. *J. Magn. Magn. Mater.* **2005**, *288*, 339. <https://doi.org/10.1016/j.jmmm.2004.09.118>.
46. Betancourt-Cantera, J.A.; Sánchez-De Jesús, F.; Bolarín-Miró, A.M.; Torres-Villaseñor, G.; Betancourt-Cantera, L.G. Magnetic properties and crystal structure of elemental cobalt powder modified by high-energy ball milling. *J. Mater. Res. Technol.* **2019**, *8*, 4995. <https://doi.org/10.1016/j.jmrt.2019.07.048>.
47. Román de Alba, J.; Martínez, J.R.; Guerrero, A.L.; Ortega-Zarzosa, G. Effect of the Silica Cover on the Properties of Co₃O₄ Nanoparticles. *Journal of Superconductivity and Novel Magnetism* **2016**, *29*, 2651. <https://doi.org/10.1007/s10948-016-3595-y>.
48. De Toro, J.A.; Andrés, J.P.; González, J.A.; Muñoz, P.; Muñoz, T.; Normile, P.S.; Riveiro, J.M. Exchange bias and nanoparticle magnetic stability in Co-CoO composites. *Phys. Rev. B* **2006**, *73*, 094449. <https://doi.org/10.1103/PhysRevB.73.094449>.
49. Williamson, G.K.; Hall, W.H. X-ray line broadening from filed aluminium and wolfram. *Acta Metall.* **1953**, *1*, 22. [https://doi.org/10.1016/0001-6160\(53\)90006-6](https://doi.org/10.1016/0001-6160(53)90006-6).
50. De, D.; Majumdar, S.; Giri, S. Spin-glass like behaviour in strongly interacting nanocrystalline Ni embedded in SiO₂. *J. Magn. Magn. Mater.* **2015**, *394*, 448. <https://doi.org/10.1016/j.jmmm.2015.06.071>.
51. De, D.; Karmakar, A.; Bhunia, M.K.; Bhaumik, A.; Majumdar, S.; Giri, S. Memory effects in superparamagnetic and nanocrystalline Fe₅₀Ni₅₀ alloy. *J. Appl. Phys.* **2012**, *111*, 033919. <https://doi.org/10.1063/1.3684624>.
52. Chattopadhyay, S.; Giri, S.; Majumdar, S. Magnetic behaviour of doped dimer compounds Sr₃Cr_{2-x}M_xO₈ (M = V, Mn). *Eur. Phys. J. B* **2012**, *85*, 4. <https://doi.org/10.1140/epjb/e2011-20660-5>.
53. Chattopadhyay, S.; Giri, S.; Majumdar, S. Broken chain effect in doped SrCuO₂. *J. Phys.: Condens. Matter* **2011**, *23*, 216006. <https://doi.org/10.1088/0953-8984/23/21/216006>.
54. Sirker, J.; Laflorie, N.; Fujimoto, S.; Eggert, S.; Affleck, I. Chain Breaks and the Susceptibility of Sr₂Cu_{1-x}Pd_xO_{3+δ} and Other Doped Quasi-One-Dimensional Antiferromagnets. *Phys. Rev. Lett.* **2007**, *98*, 137205. <https://doi.org/10.1103/PhysRevLett.98.137205>.
55. Iglesias, Ò.; Kachkachi, H. Single Nanomagnet Behaviour: Surface and Finite-Size Effects. In *New Trends in Nanoparticle Magnetism*; Springer International Publishing: Cham, Switzerland, 2021; pp. 3–38. https://doi.org/10.1007/978-3-030-60473-8_1.
56. Sánchez, E.H.; Vasilakaki, M.; Lee, S.S.; Normile, P.S.; Muscas, G.; Murgia, M.; Andersson, M.S.; Singh, G.; Mathieu, R.; Nordblad, P.; et al. Simultaneous Individual and Dipolar Collective Properties in Binary Assemblies of Magnetic Nanoparticles. *Chemistry of Materials* **2020**, *32*, 969. <https://doi.org/10.1021/acs.chemmater.9b03268>.
57. Sánchez, E.H.; Vasilakaki, M.; Lee, S.S.; Normile, P.S.; Andersson, M.S.; Mathieu, R.; López-Ortega, A.; Pichon, B.P.; Peddis, D.; Binns, C.; et al. Crossover From Individual to Collective Magnetism in Dense Nanoparticle Systems: Local Anisotropy Versus Dipolar Interactions. *Small* **2022**, *18*, 2106762. <https://doi.org/10.1002/smll.202106762>.
58. Iglesias, Ò.; Labarta, A.; Batlle, X. Exchange Bias Phenomenology and Models of Core/Shell Nanoparticles. *J. Nanosci. Nanotechnol.* **2008**, *8*, 2761. <https://doi.org/10.1166/jnn.2008.18306>.
59. Kostopoulou, A.; Brintakis, K.; Vasilakaki, M.; Trohidou, K.N.; Douvalis, A.P.; Lascialfari, A.; Manna, L.; Lappas, A. Assembly-mediated interplay of dipolar interactions and surface spin disorder in colloidal maghemite nanoclusters. *Nanoscale* **2014**, *6*, 3764–3776. <https://doi.org/10.1039/C3NR06103E>.

60. Silva, F.G.d.; Vasilakaki, M.; Cabreira Gomes, R.; Aquino, R.; Campos, A.F.C.; Dubois, E.; Perzynski, R.; Depeyrot, J.; Trohidou, K. A numerical study on the interplay between the intra-particle and interparticle characteristics in bimagnetic soft/soft and hard/soft ultrasmall nanoparticle assemblies. *Nanoscale Adv.* **2022**. <https://doi.org/10.1039/D1NA00894C>.
61. Omelyanchik, A.; Villa, S.; Vasilakaki, M.; Singh, G.; Ferretti, A.M.; Ponti, A.; Canepa, F.; Margaritis, G.; Trohidou, K.N.; Peddis, D. Interplay between inter- and intraparticle interactions in bi-magnetic core/shell nanoparticles. *Nanoscale Adv.* **2021**, *3*, 6912–6924. <https://doi.org/10.1039/D1NA00312G>.
62. Iglesias, Ò.; Batlle, X.; Labarta, A. Microscopic origin of exchange bias in core/shell nanoparticles. *Phys. Rev. B* **2005**, *72*, 212401. <https://doi.org/10.1103/PhysRevB.72.212401>.
63. Torres, F.; Morales, R.; Schuller, I.K.; Kiwi, M. Dipole-induced exchange bias. *Nanoscale* **2017**, pp. 17074–17079. <https://doi.org/10.1039/C7NR05491B>.
64. Moya, C.; Iglesias, Ò.; Batlle, X.; Labarta, A. Quantification of Dipolar Interactions in Fe_{3-x}O₄ Nanoparticles. *The Journal of Physical Chemistry C* **2015**, *119*, 24142. <https://doi.org/10.1021/acs.jpcc.5b07516>.
65. Eftaxias, E.; Trohidou, K.N. Numerical study of the exchange bias effects in magnetic nanoparticles with core/shell morphology. *Phys. Rev. B* **2005**, *71*, 134406. <https://doi.org/10.1103/PhysRevB.71.134406>.
66. Sort, J.; Langlais, V.; Doppiu, S.; Dieny, B.; Suriñach, S.; Muñoz, J.S.; Baró, M.D.; Laurent, C.; Nogués, J. Exchange bias effects in Fe nanoparticles embedded in an antiferromagnetic Cr₂O₃ matrix. *Nanotechnology* **2004**, *15*, S211. <https://doi.org/10.1088/0957-4484/15/4/017>.